DEPARTMENT OF STATISTICS
University of Wisconsin
1210 West Dayton St.
Madison, WI 53706

TECHNICAL REPORT NO. 1088

December 12, 2003

Estimating Arterial Wall Shear Stress [1]

John D. Carew [2]
Departments of Biostatistics and Medical Informatics; Statistics, University of Wisconsin, Madison, WI

Reema K. Dalal [3]
Department of Biomedical Engineering, University of Wisconsin, Madison, WI

Grace Wahba [4]
Departments of Biostatistics and Medical Informatics; Statistics, University of Wisconsin, Madison, WI

Sean B. Fain [5]
Departments of Biomedical Engineering; Medical Physics, University of Wisconsin, Madison, WI

Key Words and Phrases: arterial wall shear stress, phase constrast magnetic resonance imaging, nonparametric function estimation, Matérn covariance, reproducing kernel Hilbert space

---

[1] This paper combines two abstracts that were submitted for review to the 2004 Annual Meeting of the International Society for Magnetic Resonance In Medicine (Kyoto, Japan).

[2] Research supported in part by NIH grant T32 EY07119.
[3] Research supported in part by the UW Medical School Fund 161-9636.
[4] Research supported in part by NSF grant DMS0072292 and NIH grant EY09946.
[5] Research supported in part by the UW Medical School Fund 161-9636.

A Nonparametric Method for Estimation of Arterial Wall Shear Stress

John D. Carew, Reema K. Dalal, Grace Wahba, Sean B. Fain

INTRODUCTION

Arterial wall shear stress (WSS) is proportional to the derivative of blood velocity evaluated at the arterial wall. One method for noninvasively estimating WSS is through post-processing of phase contrast magnetic resonance images (PC-MRI). PC-MRI is capable of measuring blood velocity along the direction of arterial blood flow [1]. Parametric methods for estimating WSS from PC-MRI depend on assumptions such as approximately circular vessel symmetry or laminar flow [2]. This abstract proposes a nonparametric method for estimating WSS from PC-MR images for more general application of WSS estimation to more complex vessel geometries and flow regimes.

MATERIALS AND METHODS

Method: The WSS estimation method consists of: (1) determination of the vessel wall position, (2) fitting of a nonparametric function to the blood velocity measurements within the vessel, (3) approximation of the derivative of the blood velocity function at the boundary. Specifically, in step 1, the vessel interior wall pixels are automatically extracted from a magnitude image with an edge detection algorithm [3]. A closed, periodic smoothing spline curve is then fit to the boundary pixels to estimate the vessel wall at sub-pixel resolution and to compute the normal directions. Pixels from the PC-MR image that are within the boundary are segmented for fitting. In step 2, interior points are denoted as (x_i, y_i, z_i) for $i = 1, \ldots, n$, where x_i and y_i indicate pixel location and z_i indicates the corresponding velocity. Blood velocity is modeled as $z_i = f(x_i, y_i) + \epsilon_i$, where $\epsilon_i \sim_{iid} \mathcal{N}(0, \sigma^2)$, where we assume only that f is a smooth function. An estimator for f is found in a reproducing kernel Hilbert space denoted $\mathcal{H}_R$ with reproducing kernel R such that

$$\hat{f}(x, y) := \arg\min_{f \in \mathcal{H}_R} \left(\sum_{i=1}^{n} (z_i - f(x_i, y_i))^2 + \lambda ||f||^2_{\mathcal{H}_R} \right)$$

The unique solution follows from a more general result in [4] and involves a linear combination of the reproducing kernel evaluated at a point $t := (x, y)$ and the data, namely

$$\hat{f}(t) = \sum_{i=1}^{n} \mathbf{c}_i R(t, t_i),$$

where

$$\begin{aligned} \mathbf{c} &:= (\mathbf{\Sigma} + \lambda \mathrm{I})^{-1} (z_1, \ldots, z_n)', \\ \mathbf{\Sigma} &:= [R((x_i, y_i), (x_j, y_j))]_{ij}, \quad i, j = 1, \ldots, n. \end{aligned}$$

The function $R(\cdot, \cdot)$ provides a model for spatial covariance and matrix $\mathbf{\Sigma}$ can be regarded as a spatial covariance matrix. In fact, R, which is a symmetric positive definite function, defines a

unique $\mathcal{H}_R$. Here, R is selected from the Matern family of radial basis functions [5]. Let $\tau := ||(x_i, y_i) - (x_j, y_j)||$ be the Euclidean distance between two points. Then $R_\nu(\tau) := \exp(-\tau)\pi_\nu(\tau)$, $\nu = 0, 1, 2, \ldots$ is the Matern reproducing kernel for order ν, where π_ν is a polynomial of a particular form [5]. The regularization parameter π and order ν can be objectively determined with generalized cross-validation [6]. In step 3, the estimated velocity function is used to evaluate the derivative at the boundary along the normal directions, which yields the wall shear rate (WSR). WSS is the product of the blood viscosity and WSR.

Experiment: A glass tube phanton was constructed with an indentation to provide a nonconvex cross-section. The phantom experiment was performed on 1.5 T Signa LX (GE Medical systems, Milwaukee, WI) scanner using a 2D phase contrast (PC) sequence. The glass tube was connected to a Cole-Parmer pump placed outside the scanner. The flow rate was set to 6.25 ml/s. The parameters used for the scan were FOV: 80 mm x 80 mm, matrix size: 512×512, NEX: 10, TR: 29 ms, Flip angle: 15 degrees, and slice thickness: 0.7mm.

RESULTS

The proposed method was successfully applied to the phantom data even in the concave region of the phantom where parametric methods that depend on convexity or symmetry assumptions would typically fail. The boundary pixels determined by the Canny method are marked on the magnitude image in Figure 1. The estimated velocity function along with contours is in Figure 2. A regularization parameter of $\lambda = 1250$ and Matern order $\nu = 4$ were used to estimate the velocity function. Notice that the contours are more closely spaced near the indentation than in other regions of the tube. This indicates a greater rate of velocity change and, hence, greater wall shear stress. The estimated derivatives are plotted versus angle in Figure 3. The angle is with respect to the center of the tube and increases counter clock-wise. There is a systematic trend in the estimates that reflects the shape of the tube. Note the large WSS between angles 4 and 5 radians. This is the region of the tube where the indentation is greatest.

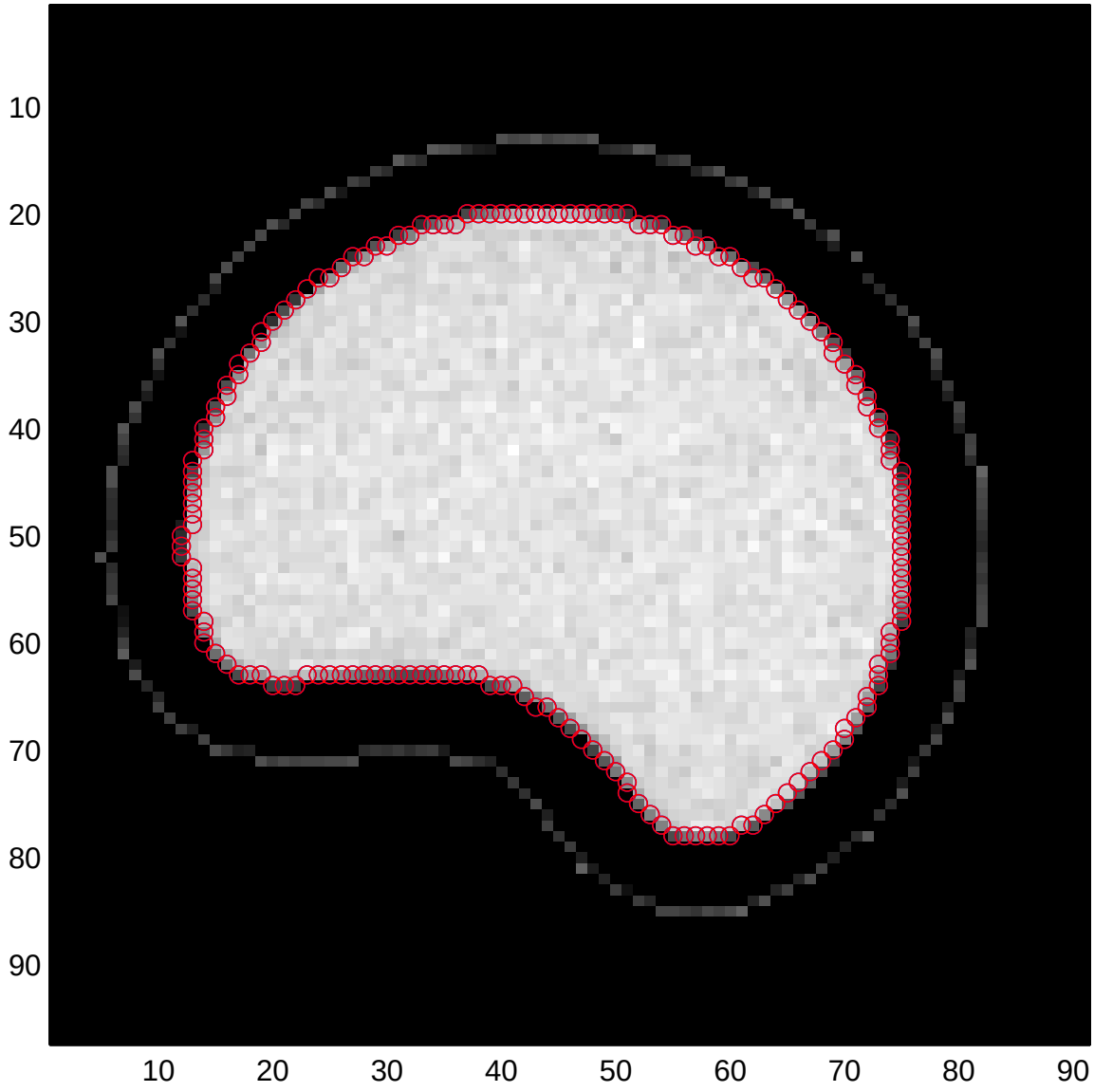

Figure 1: The magnitude image shows the cross-sectional shape of the glass tube. Boundary pixels that were automatically identified by the Canny method are indicated in red. These pixels intersect the glass tube's interior wall.

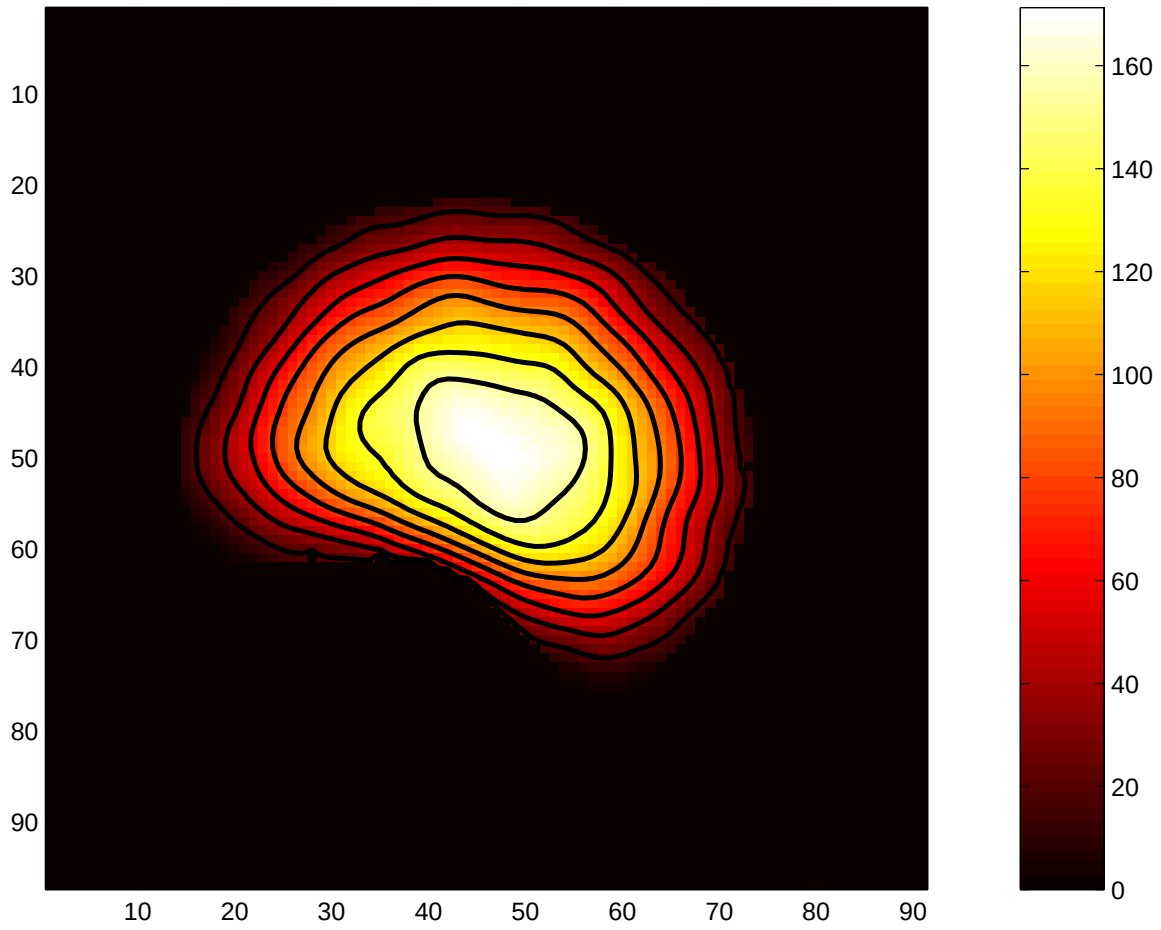

Figure 2: The image shows a nonparametric fit of the cross-sectional fluid velocity in the direction perpendicular to the plane of the paper. A Matern order $\nu = 4$ and a smoothing parameter $\lambda = 1250$ were used in this estimate of the velocity function. Relatively closely-spaced contour lines near the tube indentation indicate a relatively high wall shear stress near the indentation.

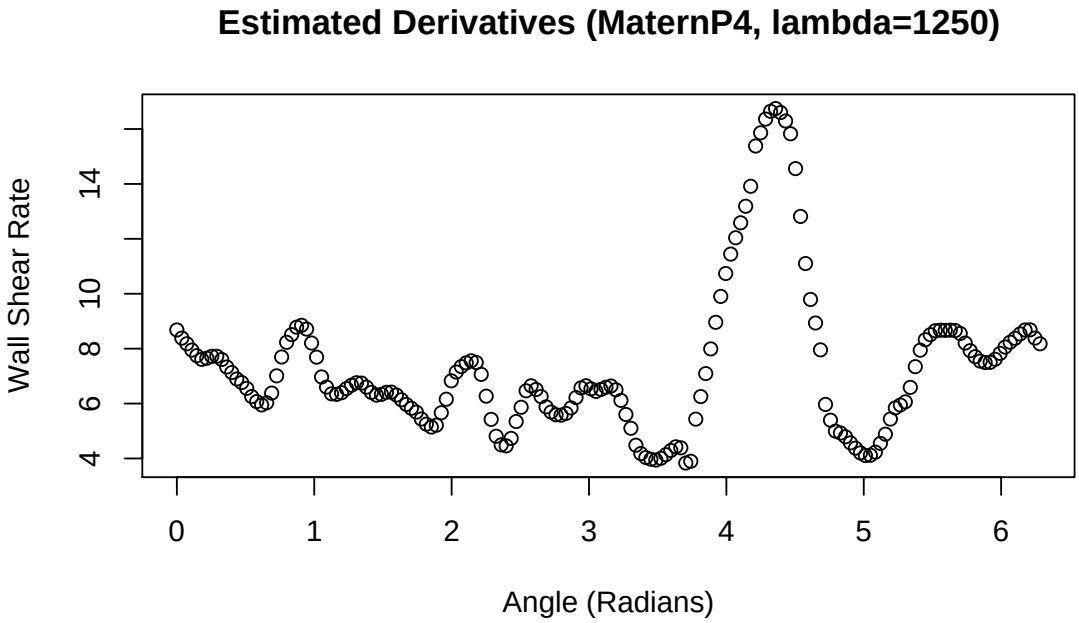

Figure 3: A plot of the estimated wall shear rate versus angle shows systematic variation. In regions of the tube near the indentation (roughly, 4 to 5 radians), the wall shear rate is greatest.

DISCUSSION

The main result of this abstract is to describe a nonparametric method and establish its feasibility for estimating WSS in blood vessels. Nonparametric function estimation in $\mathcal{H}_R$ does not require restrictive assumptions about the form of the blood velocity profile or symmetry of the vessel. In the phantom data, this method produced a good fit and sensible estimates of WSR along the entire vessel wall. While the Canny method was able to automatically identify boundary pixels from the phantom data, determining vessel boundaries in vivo might be more difficult. Others have shown the advantages of double inversion black blood MRI for identifying vessel boundaries [7]. One limitation of this study is the lack of a gold standard to confirm the WSR estimates. Measuring WSR with additional methods would provide confirmational evidence. While not considered in this abstract, the bootstrap is a procedure that can be used to estimate confidence intervals or standard errors for the WSS estimates. This method can also be extended to fit 3D images or a series of contiguous 2D images acquired along the flow direction. Additional phantom studies and in vivo studies are necessary to provide better understand the strengths and limitations of this nonparametric method and how they compare to other methods. The preliminary results from this study suggest the promise of the nonparametric method as a potential diagnostic tool.

References

[1] Pelc NJ, Bernstein MA, Shimakawa A, Glover G. (1991). *J Mag Reson Imag* 1:405-423.

[2] Oyre S, Ringgaard S, Kozerke S, et al. (1998). *Magn Reson Med* 40:645-655.

[3] Canny J. (1986). *IEEE J Pattern Analysis Machine Intelligence* 8(6): 679-698.

[4] Kimeldorf G, Wahba G. (1971). *J Math Anal Appl* 33:82-95.

[5] Stein ML. (1999). *Interpolation of Spatial Data: Some Theory for Kriging*. Springer-Verlag, New York.

[6] Wahba G. (1990). *Spline Models for Observational Data* . SIAM, Philadelphia.

[7] Steinman DA, Thomas JB, Ladak HM, et al. (2002). *Magn Reson Med* 47:149-159.

Recovering the Boundary of an Object in an Image

John D. Carew, Grace Wahba, Reema K. Dalal, Sean B. Fain

INTRODUCTION

A common problem in imaging is to recover the cross-sectional boundary of an anatomical structure or object in an image. Identifying the pixels that intersect the boundary may not be sufficient for some applications, particularly when sub-pixel resolution is necessary. Fitting a functionally defined closed, parametric curve to boundary pixels would provide arbitrary resolution and allow calculation of boundary tangents and normals. In particular, to erode or shrink an object boundary, points need to be translated along the normal direction. One specific application where these methods are necessary is arterial wall shear stress estimation. The purpose of this abstract is to propose and illustrate a method to recover the boundary of an object from a set of boundary pixels.

MATERIALS AND METHODS

A parametric planar curve $\mathcal{C} := (x(t), y(t))$ for $t \in [a, b]$ maps the interval $[a, b]$ into the plane. Assume that the component functions $x(t)$ and $y(t)$ have continuous derivatives. The parameter t gives an ordering to points on the curve. A closed curve is periodic with period ω if points t and $t + r\omega$ map to the same points on $\mathcal{C}$ for all integers r. Fitting a closed, parametric curve to image data involves fitting the component functions $x(t)$ and $y(t)$ from a set $\mathcal{P}$ of pixels with coordinates (x_i, y_i) for $i = 1, \ldots, n$. The method consists of: (1) identifying the boundary pixels, (2) parameterizing the pixels, and (3) fitting a smoothing spline to each of the coordinates. In the first step, boundary pixels can be identified by any method that is most appropriate for the given image. Here, the Canny method [1] for automatic edge detection was used. For step 2, it is assumed that the true object boundary encloses a topologically star-shaped set. Then, the mean of $\mathcal{P}$ lies inside of the boundary. The set $\mathcal{P}$ is then shifted so that it has mean zero. The points are then converted to polar coordinates and sorted by increasing angle. This defines an ordering of the pixels along the curve. Then, to assign a t_i to each (x_i, y_i), t_i is selected such that $t_{i+1} - t_i$ is proportional to the distance between (x_i, y_i) and (x_{i+1}, y_{i+1}). In step 3, a periodic cubic smoothing spline [2] is independently fit to (t_i, x_i) and (t_i, y_i) pairs, respectively. As an illustration, this method is applied to a phantom magnitude image acquired from a phase contrast MRI pulse sequence on a standard 1.5T clinical scanner. The fitted spline curve is used to compute the boundary normal lines and subsequently translate boundary points inward to yield an eroded boundary.

RESULTS

The boundary detection method was able to successfully fit a curve to the boundary points. The phantom image is in Figure 4. Canny edge detection worked well for this image. Plots of the parameterized boundary pixel coordinates versus parameter are given in Figure 5 and Figure 6,

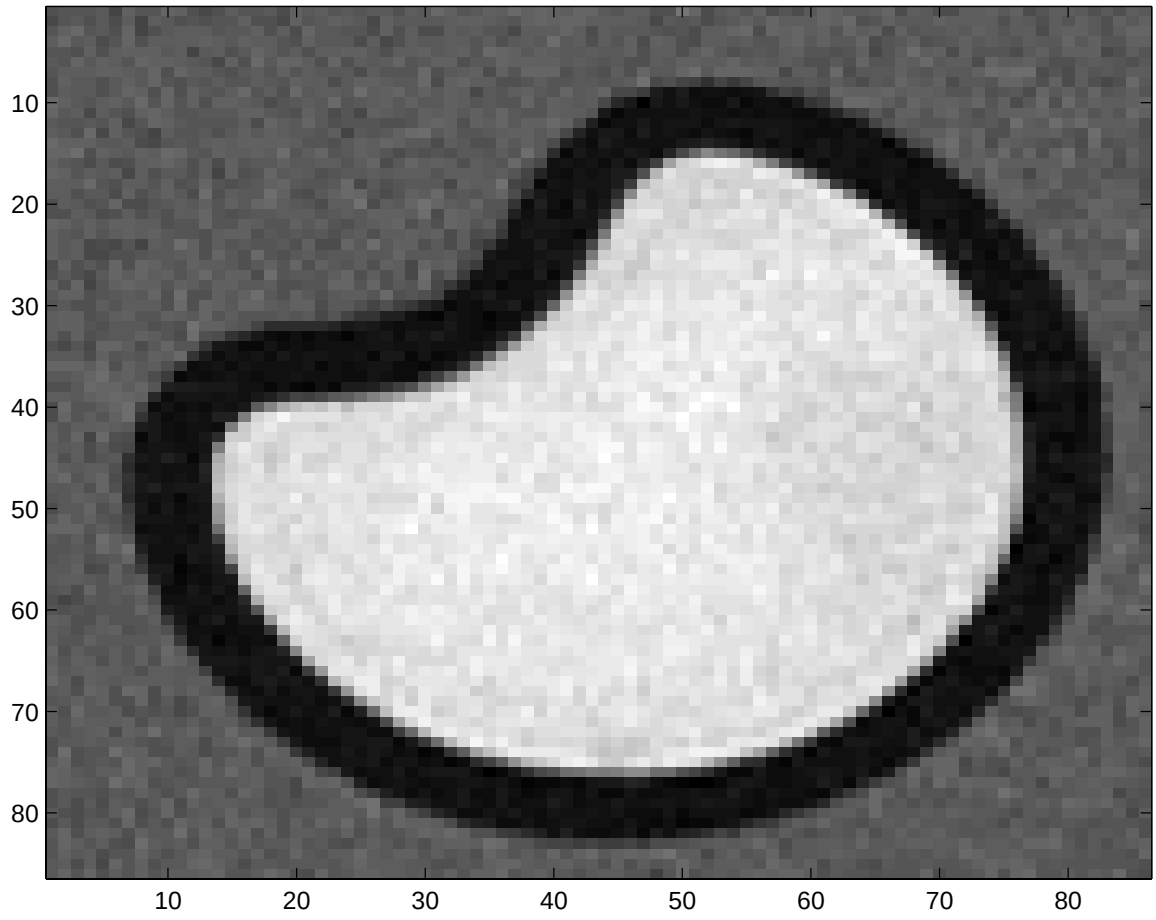

Figure 4: This is a magnitude image of a cross-section of a glass tube acquired from a phase contrast MRI pulse sequence. Boundary pixels are identified from this image with an edge detection algorithm.

respectively. Note that these plots appear similar to sine and cosine, which indicates the approximate circularity of the boundary. In Figure 7, a plot of the smoothing spline curve is given with the boundary pixel coordinates. The interior points are an erosion of the boundary in the normal direction. The eroded points preserve the boundary shape.

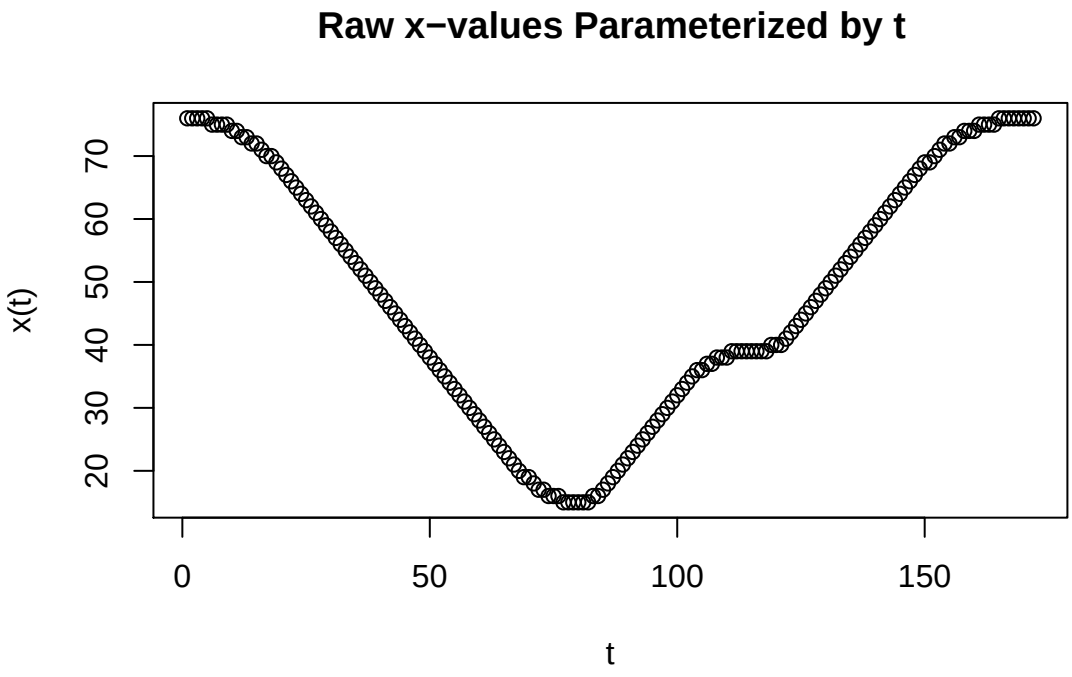

Figure 5: The raw x_i coordinates of the boundary pixels are plotted against their parameter t_i. The parameter defines an order to the boundary pixels.

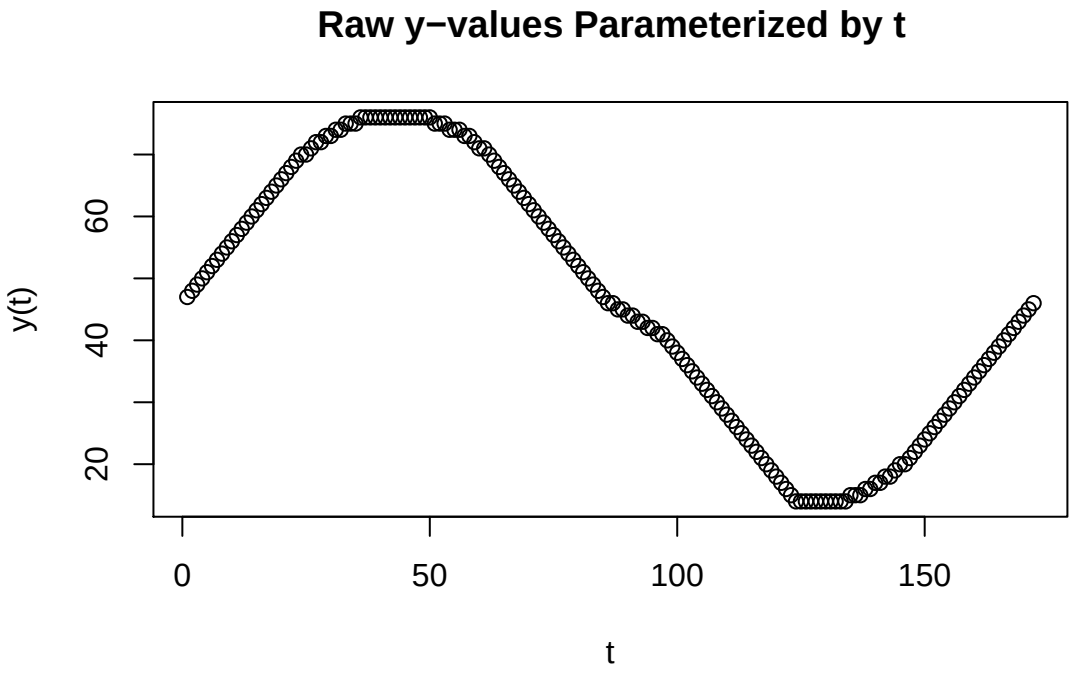

Figure 6: The raw y_i coordinates of the boundary pixels are plotted against their parameter t_i.

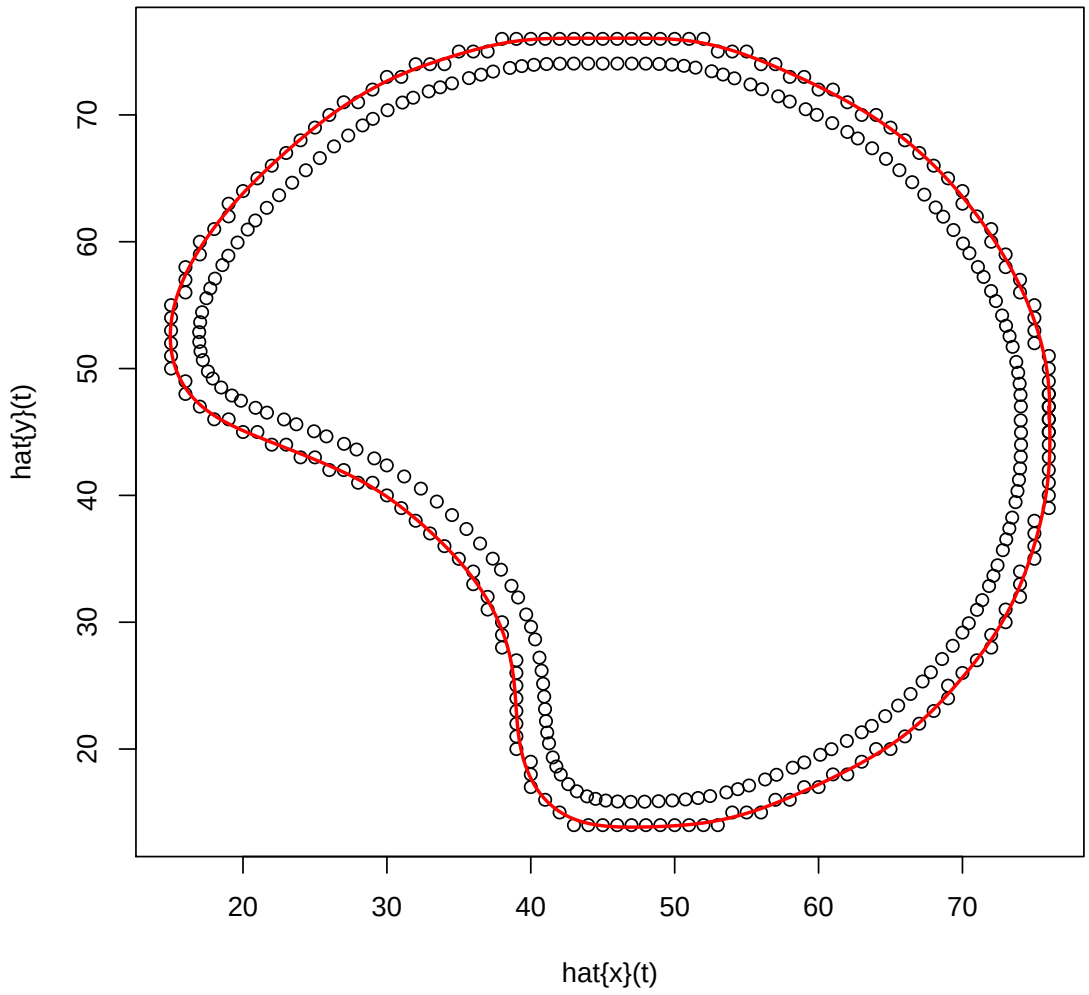

Figure 7: The red curve is a smoothing spline fit to the boundary pixel locations. The interior points are an erosion of the fitted boundary points. Notice that the spline curve recovers the boundary and that the boundary erosion preserves shape.

DISCUSSION

This abstract describes a method for estimating a closed parametric curve from a set of boundary points. The smoothing spline curve gives a functionally defined boundary that provides arbitrary resolution. The smoothing yields a curve that does not interpolate the pixel coordinates. Instead it follows the natural contours of the object boundary, which results in a more realistic representation of the actual boundary. One limitation of this method is the need to define an ordering of the pixels along the boundary for the purposes of parameterization. For objects that are not star-shaped, it will not be possible to convert to polar coordinates and order by angle. However, it is suspected that the smoothing spline will still work provided that the boundary points can be parameterized by other means. Applications of this method to more complicated images will provide additional insights on its strengths and limitations.

REFERENCES

[1] Canny J. (1986). *IEEE J Pattern Analysis Machine Intelligence* 8(6): 679-698.

[2] Wahba G. (1990). *Spline Models for Observational Data.* SIAM, Philadelphia.